Theoretical study of vesicle shapes driven by coupling curved proteins and active cytoskeletal forces (Supplementary Information)

Miha Fošnarič, Samo Penič, Aleš Iglič, Veronika Kralj-Iglič, Mitja Drab and Nir Gov

S1: A theoretical model of self-assembly of curved nanodomains in a two-component membrane

We use the theory of self-assembly to describe the accumulation of curved membrane nanodomains composed of lipids and proteins into spherical or necklace membrane protrusions. The curved nanodomains (of total number N) are initially distributed in the weakly curved spherical membrane surface of constant mean curvature $H{=}1/R_0$. We assume that the nanodomains are laterally mobile over the membrane surface. For isotropic curved membrane protrusion of constant high mean curvature $H{=}1/r$. Here, r is the radius of curvature everywhere on the membrane protrusion which may be a sphere or necklace formation (see Fig. S1) and assume $R_0 > r$.

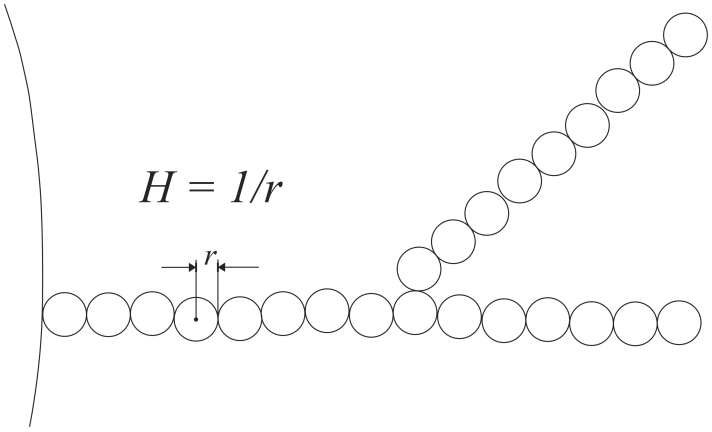

Figure S1 Growth of necklace-like protrusions is energetically favorable when critical concentration $\tilde{x}_c$ is surpassed.

For the sake of simplicity we assume that the free energy of a single flexible membrane nanodomain can be written in the form [V. Kralj-Iglič et al. Deviatoric elasticity as a possible physical mechanism explaining collapse of inorganic micro and nanotubes, Physics letters A, 2002]:

$$f = \frac{\xi}{2}(H - H_0)^2 a_o \,. \tag{S1}$$

where H_0 is the intrinsic mean curvature of an isotropic membrane nanodomain, ξ is the elastic constant and a_0 is the area per single nanodomain. In aggregates of curved flexible membrane nanodomains the local membrane bending constant is $k_c = \xi/4$ and the membrane spontaneous curvature $c_0 = 2H_0$.

Curved flexible membrane nanodomains in aggregates interact with neighbouring membrane nanodomains. We denote the corresponding interaction energy per curved flexible membrane nanodomain (monomer) in an aggregate composed of i nanodomains as $w(i)$ where we assume that the energy $w(i)$ depends on the size of the aggregate composed of i nanodomains. The mean free energy per nanodomain in a curved aggregate (where $H = D = 1/r$) composed of i nanodomains can be written as:

$$\mu_i = f_c - w(i)\,, \tag{S2}$$

where $f_c = f(H{=}1/r)$ and $w(i) > 0$. We assume that in the weakly curved spherical regions of the membrane (having $H{=}1/R_0$) the concentration of nanodomains is always below the critical aggregation concentration and therefore nanodomains cannot form two-dimensional flat aggregates. The mean energy per nanodomain in the weakly curved membrane regions is $\tilde{\mu}_1 = f_{sp}$, where $f_{sp} = f(H{=}1/R_o)$. The number density of curved proteins in the weakly curved membrane regions is

$$\tilde{x}_1 = \frac{\tilde{N}_1}{M}\,, \tag{S3}$$

where $\tilde{N}_1$ is the number of monomeric curved nanodomains in the weakly curved membrane regions and M is the number of lattice sites in the whole system. The distribution of highly curved aggregates in the membrane protrusions on the scale of number density is expressed as

$$x_i = \frac{iN_i}{M}\,, \tag{S4}$$

where N_i denotes the number of aggregates with aggregation number i. The number densities $\tilde{x}_1$ and x_i must fulfil the conservation condition for the total number of flexible nanodomains in or on the membrane:

$$\tilde{x}_1 + \sum_{i=1}^{\infty} x_i = N/M. \tag{S5}$$

The free energy $\mathscr{F}$ of all nanodomains in or on the membrane can be written as:

$$\mathscr{F} = M[\tilde{x}_1\ \tilde{\mu}_1 + kT\tilde{x}_1(\ln\tilde{x}_1 - 1)] + M\sum_{i=1}^{\infty}\left[x_i\ \mu_i + kT\frac{x_i}{i}\left(\ln\frac{x_i}{i} - 1\right)\right] - \mu M(\tilde{x}_1 + \sum_{i=1}^{\infty} x_i)\ , \tag{S6}$$

where μ is the Lagrange parameter assuring conservation of protein concentrations. The above expression for the free energy also involves the contributions of configurational entropy. We minimize $\mathscr{F}$ with respect to $\tilde{x}_1$ and x_i:

$$\frac{\partial\mathscr{F}}{\partial\tilde{x}_i} = 0\,, \frac{\partial\mathscr{F}}{\partial x_i} = 0,\ i = 1, 2, 3, \ldots, \tag{S7}$$

which leads to equilibrium distributions:

$$\tilde{x}_1 = \exp\left(-\frac{f_{sp} - \mu}{kT}\right), \tag{S8}$$

$$x_i = i\ \exp\left(-\frac{i}{kT}\left[f_c - w - \mu\right]\right), \tag{S9}$$

where we assumed for simplicity that $w(i) = w$ is independent of aggregate size. The quantity μ can be expressed from Eq. S8 and substituted in Eq. S9 to get:

$$x_i = i\ \left[\tilde{x}_1 \cdot \exp\left(\frac{f_{sp} + w - f_c}{kT}\right)\right]^i. \tag{S10}$$

We see that if the concentration $\tilde{x}_1$ is small, aggregate growth will not be favorable, since $x_1 > x_2 > x_3 \ldots$. Furthermore, x_i can never exceed unity, leading to the maximal possible value of the number density of monomeric curved flexible nanodomains in the weakly curved parts of the membrane when $\tilde{x}_1$ approaches $\exp\left[(f_c - f_{sp} - w)/kT\right]$. The critical concentration is therefore

$$\tilde{x}_c \approx \exp\left(\frac{\Delta f - w}{kT}\right), \tag{S11}$$

where $\Delta f = f_c - f_{sp}$ is the difference between the energy of a single nanodomain on the highly curved membrane protrusion and the energy of the single nanodomain in the weakly curved membrane region with:

$$\Delta f = \frac{\xi a_o}{2r}\left(\frac{1}{r} - 2H_0\right) - \frac{\xi a_o}{2R_0}\left(\frac{1}{R_0} - 2H_0\right). \tag{S12}$$

If $\tilde{x}_1$ is above $\tilde{x}_c$, the formation of a very long necklace membrane protrusions composed of curved membrane proteins is energetically favourable. It can be seen from Eq. S11 that longitudinal growth of the necklace membrane protrusions is dependent on the energy difference Δf (Eq. S12) and the strength of the direct interaction between nanodomains w. The critical concentration $\tilde{x}_c$ strongly depends on H_0.

In the approximation limit $R_0 \gg r$ we can rewrite Eq. S12 as:

$$\Delta f \simeq \frac{\xi}{2r}\left(\frac{1}{r} - 2H_0\right) = \frac{2k_c}{r}\left(\frac{1}{r} - c_0\right), \tag{S13}$$

where k_c and c_0 are the local bending constant and spontaneous curvature of aggregates of nanodomains, respectively. We may rewrite Eq. S11:

$$\tilde{x}_c \approx \exp\left(\ 2\ \frac{k_c}{kT}\ \frac{a_o}{r^2}\,(1 - c_0 r) - \frac{w}{kT}\right). \tag{S14}$$

For $1 < c_0 r$ the value of Δf is always negative. The theoretically predicted existence of necklace membrane protrusions (without application of the local forces) within the self-assembly theory is in line with our MC predictions.

Since the density of nanodomains in or on the membrane is defined with the conservation condition (Eq. S5), this also gives us the relation between normalized temperature T/T_0 and total curved nanodomains concentrations $\rho = N/M$. Using the parameters from the MC simulations, we may graph dependencies $x_i(i)$, as seen in Fig. S2. Above small concentrations and especially above $\tilde{x}_c$, aggregates start to form, where the peaks of the distributions are strongly dependent on the total protein concentration in the lattice. We see that the critical line beyond which aggregate growth is favourable agrees well with the results of MC simulations.

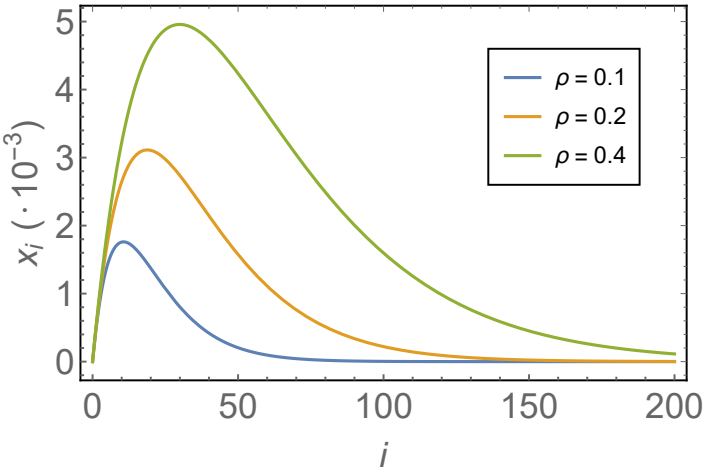

Figure S2 Aggregate concentrations in dependence on number of nanodomains in the aggregate for different number of flexible nanodomains on the membrane.

S2: A theoretical analysis of the critical cluster size that enables tubular shapes for flat active proteins

The conditions that trigger the transition into the tubular-shapes (Fig.7) are given by the following force balance:

The force applied at the tip of the cylindrical protrusion by the cluster of active proteins is

$$F_a = F\frac{\pi R^2}{a}, \tag{S15}$$

where F is the force per active protein, R is the radius of the cylinder, and a is the area of a protein on the membrane.

This is balanced by the restoring force of the membrane bending energy

$$F_b = \kappa\frac{2\pi}{R}, \tag{S16}$$

with κ the bending modulus. The force balance gives the radius of the cylindrical protrusions in this phase of the vesicle shapes

$$R_c = \left(\frac{2\kappa a}{F}\right)^{1/3}. \tag{S17}$$

The prediction of Eq. S17 is in good agreement with simulations (see Fig. S3), where we took for a the area that corresponds to one vertex in a hexagonal mesh, $a = \sqrt{3}l_0^2/2$, where $l_0 = (l_{min} + l_{max})/2$.

In the phase of tubular shapes, there are several protrusions (typically 2-3) that pull in opposite directions to provide an approximate overall force balance, and maintain the relative stability of this shape. Some fusions of protrusions do occur, especially for cases with a larger number of thinner protrusions, so that their number fluctuates.

An alternative to the derivation of the estimate of the protrusion's width given above can be obtained as follows: the total work done by the active forces that pull and extend a protrusion of length L, combined with the curvature energy, is given by

$$W = \frac{\pi R^2}{a}FL + 2\pi RL\frac{\kappa}{2}\frac{1}{R^2}, \tag{S18}$$

where we assume that the cylinder is very long compared to its radius, so that its surface area is given by: $A \simeq 2\pi RL$. For a fixed area constraint, such that we can substitute $L = A/(2\pi R)$, we can rewrite this work function as

$$W = \frac{RF}{2a}A + A\frac{\kappa}{2}\frac{1}{R^2}. \tag{S19}$$

Differentiating this work with respect to R we find that the minimum is given by the radius of Eq. S17.

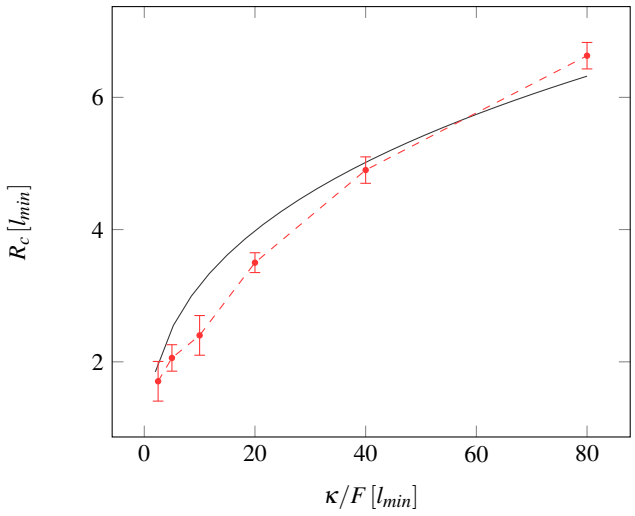

Figure S3 Radius of cylindrical protrusions as a function of the κ to F ratio for the system with almost flat active proteins with parameters $c_0 = 1/(0.9l_{\min})$, $\rho = 11\%$, $w = 1kT_0$ and $T/T_0 = 0.7$ (see top-left hydra-like snapshot on Fig. 7d). Black solid curve is the prediction of Eq. S17, while red dots are the results of the simulations with error bars indicating standard errors.

SI3: Cluster size dependence on the strength of the direct interaction for active system

See Fig. S4.

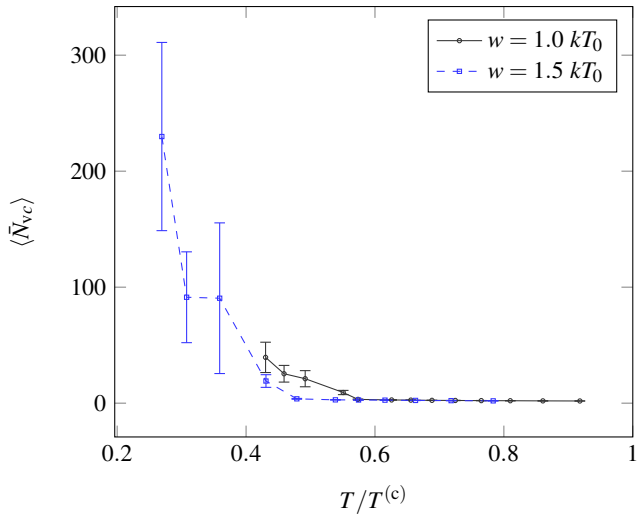

Figure S4 Mean cluster size $\langle \bar{N}_{vc} \rangle$ as a function of $T/T^{(c)}$ for two different values of the direct interaction constant (legend), for an active system with $F = 1\,kT_0/l_{min}$. The average protein density is $\rho = 9.5\%$. The graphs do not collapse, unlike in the passive system (Fig. 2d).

SI4: Testing for hysteresis of the pancake transition

See Fig. S5.

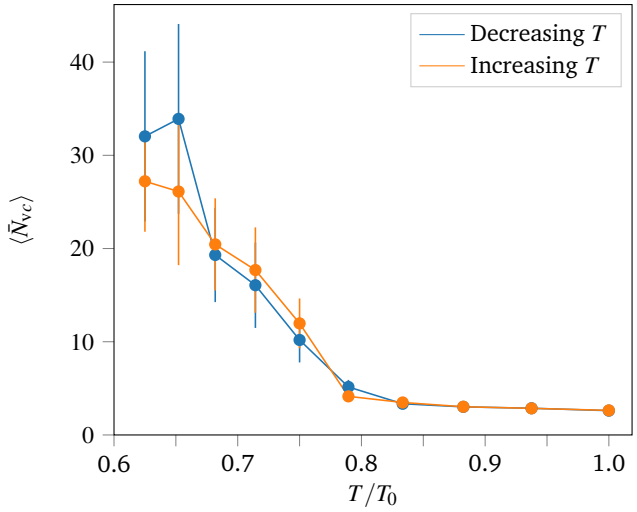

Figure S5 Hysteresis test for the transition into the pancake shape (corresponding to the system shown in Figs. 3,4), showing ensemble averaged mean cluster size for active curved proteins as a function of temperature for two different initial states – above (blue) and below (red) pancake transition. Average protein density is $\rho = 11\%$. Error bars denote standard deviations.

SI5: Cluster size dependence on the density

The activity-driven transition is clearly seen in Fig. 4b of the main text – in the mean cluster size $\langle \bar{N}_{\rm vc} \rangle$ as a function of temperature T/T_0 for different average densities of proteins ρ. Without the active protrusive force, $\langle \bar{N}_{\rm vc} \rangle$ monotonically increases with ρ and decreases with T, while the protrusive force gives rise to the sharp transition into pancake-like shapes. The lower stability of the rim aggregate at high protein densities, that we already noticed in Fig.3, is manifested in the non-monotonic dependencies of $\langle \bar{N}_{\rm vc} \rangle$ on ρ and T (Fig. S6).

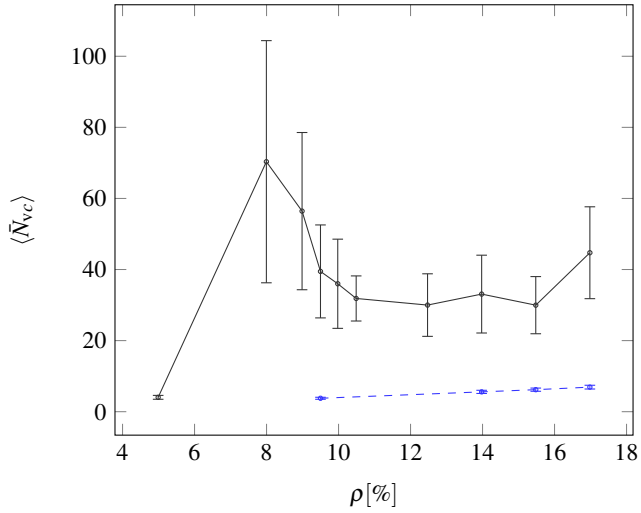

Figure S6 Ensemble averaged mean cluster size as a function of the average density of curved proteins with $c_0 = 1/l_{\rm min}$. Results with active protrusive force $F = 1\,kT_0/l_{\rm min}$ are shown for $T/T_0 = 0.625$ (solid) and without it for $T/T_0 = 0.4$ (dashed).

SI6: Vesicle size dependence of the budding and pancake transition

The dependence of the pancake transition on the vesicle radius mirrors the effect on the overall cluster size distribution: a smaller vesicle has smaller protein clusters and a lower transition temperature (Fig. S7).

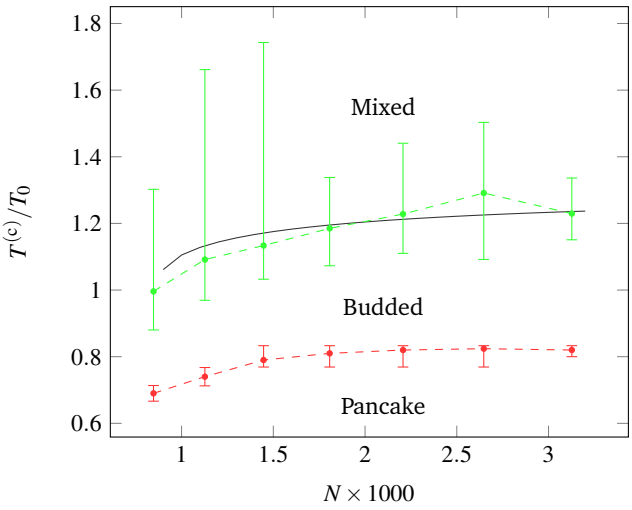

Figure S7 Dependence of the budding (green) and pancake (red) transition curves as functions of the number of vertices composing the vesicle with $F = 1\,kT_0/l_{\min}$,$c_0 = 1/l_{\min}$, $\rho = 9.5\%$. Spherical vesicle with the same membrane area A has the radius $R_0 \approx 0.35\sqrt{N}$ (in units of $l_{\min}$). Black solid curve is the prediction for the budding transition line from the linear stability analysis.

SI7: Osmotic pressure dependence of the pancake transition

We studied the effects of adding an isotropic osmotic pressure, which adds a term of the form $-p \cdot V$ to the energy of the vesicle.

We begin by estimating the pressure that balances the active forces of the active proteins along the circular rim of the pancake shape. The work done by the active proteins and the osmotic pressure is

$$W \simeq -p\pi R^2 d + \frac{\pi R d}{a} F R, \tag{S20}$$

where we treat the pancake as very thin compared to its radius ($d \sim 1/c_0 \ll R$), so that its volume $V \simeq \pi R^2 d$. We keep the membrane area constant, so maintain: $A = 2\pi R(d+R)$. Substituting this constraint into Eq. S20, we find a critical pressure that balances the protein forces, when $p_c \sim F/a \sim kT_0/l_{min}^3$. At higher pressures, the isotropic pressure overwhelms the protein active forces, and prevents the pancake shapes.

However, as we can see from the phase diagram on Figs. S8 to S13 (details of the simulations are descibed below), we find that there is significant shrinkage of the pancake phase already at much lower pressures. We can explore the interplay between the osmotic pressure, the pancake shape and the bending energy that keeps the circular protein cluster along the highly curved rim. By considering only the bending energy and work done by the osmotic pressure, we write an energy functional

$$W \simeq -p\pi R^2 d + \frac{\pi R d}{2} \kappa \left(\frac{1}{2} \left(\frac{1}{R} + \frac{2}{d} \right) - c_0 \right)^2. \tag{S21}$$

Since we are interested in a regime of low pressures, where the pancake becomes thicker but still maintains $d \ll R$, we can simplify the mean curvature

$$W \simeq -p\pi R^2 d + \frac{\pi R d}{2} \kappa \left(\frac{1}{d} - c_0 \right)^2. \tag{S22}$$

Minimizing this functional, while maintaining the constant surface condition, provides the steady-state width and radius, for a given surface area A. It turns out that we can approximate R as constant, since it changes very little, and the steady-state width can be approximated as

$$d \simeq \sqrt{\frac{\kappa}{c_0^2 \kappa - pR}}. \tag{S23}$$

Plugging this width into the bending energy of the proteins at the rim (second term in Eq.S22), and equating this bending energy to some threshold value δE (of order kT) at which the proteins can be thermally activated to leave the highly curved rim, we get for the critical pressure the expression

$$p_c' \simeq 2\sqrt{\frac{\kappa}{R^3}} \sqrt{c_0^3 \delta E}. \tag{S24}$$

Using the values of our simulations in Fig. S14, and noting that the change in the bending energy of proteins at the transition is of the order $\delta E \sim 0.07\,kT$ (see Fig. S15), this critical pressure is: $p_c' \sim 0.01\,kT_0/l_{min}^3$, which is close to the values that we found to affect the pancake transition temperature.

In the simulations in the main text the membrane is (almost) tension free. However by including the osmotic pressure, we can expect the membrane tension to increase. To evaluate for membrane tension, we added to the hamiltonian for the membrane energy, besides the $-pV$ energy term, also the term for tension energy:

$$W_A = \frac{k_A}{2} \sum_{i=1}^{N_t} \left(\frac{a_i}{a_0} - 1 \right)^2, \tag{S25}$$

where k_A is the elastic constant of the membrane and the sum runs over all of N_t triangles of the network, a_i is area of triangle i, and a_0 is area of a tensionless triangle. For a_0 we choose area of the equilateral triangle, $a_0 = \sqrt{3}\, l_0^2/4$, with side lengths $l_0 = (l_{min} + l_{max})/2$. We define membrane tension as the average tension energy per membrane area,

$$\sigma = \left\langle \frac{W_A}{A} \right\rangle, \tag{S26}$$

where A is area of the membrane for a given microstate and bra–ket denote canonical ensemble average.

From Fig. S14 we see that for no osmotic pressure, $p = 0$, membrane tension is around $0.0212\,kT_0/l_{\min}^2$. As can be seen by comparing the phase diagram in Fig. 3 with Fig. S8, we can see that, as expected, the tension term (Eq. S25) does not change the behavior of the system for $p = 0$. When we introduce the osmotic pressure, the pancake protein rim disassembles (on Fig. S14 at $p \approx 0.0065\,kT/l_{\min}^3$) while the membrane tension is still close to the value at $p = 0$. Near the border of the pancake phase, the behavior is quite dynamic, the protein aggregate at the rim can disassemble and reassemble, and with that the vesicle shape looses and gains again the pancake-like shape (see Movies S4 and S5). At larger osmotic pressures (on Fig. S14 for $p > 0.01\,kT/l_{\min}$), the pressure difference starts to dominate the behavior, the vesicle swells and membrane tension starts to increase (see Fig. S14).

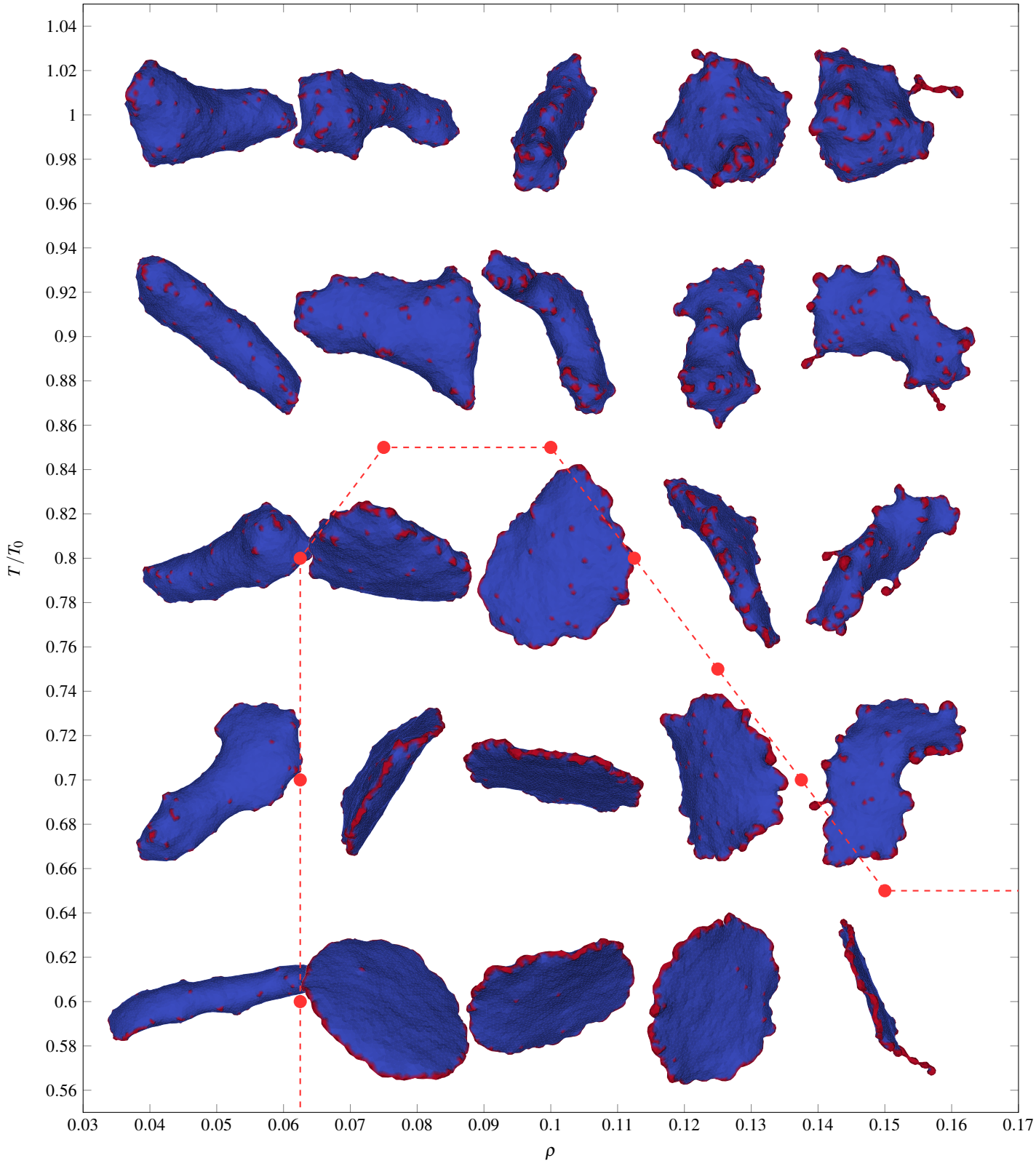

Figure S8 Representative snapshots of the vesicle at protein densities $\rho = 5$, 7.5, 10, 12.5 and 15% and temperatures $T/T_0 = 0.6$, 0.7, 0.8, 0.9 and 1.0, for $p = 0$ (with $k_A = 1\,kT_0$, $w = 1\ kT_0$ and $F = 1\,kT_0/l_{min}$). Approximate temperatures below which a transition into a pancake-like shapes is observed are indicated with red dots connected with dashed lines.

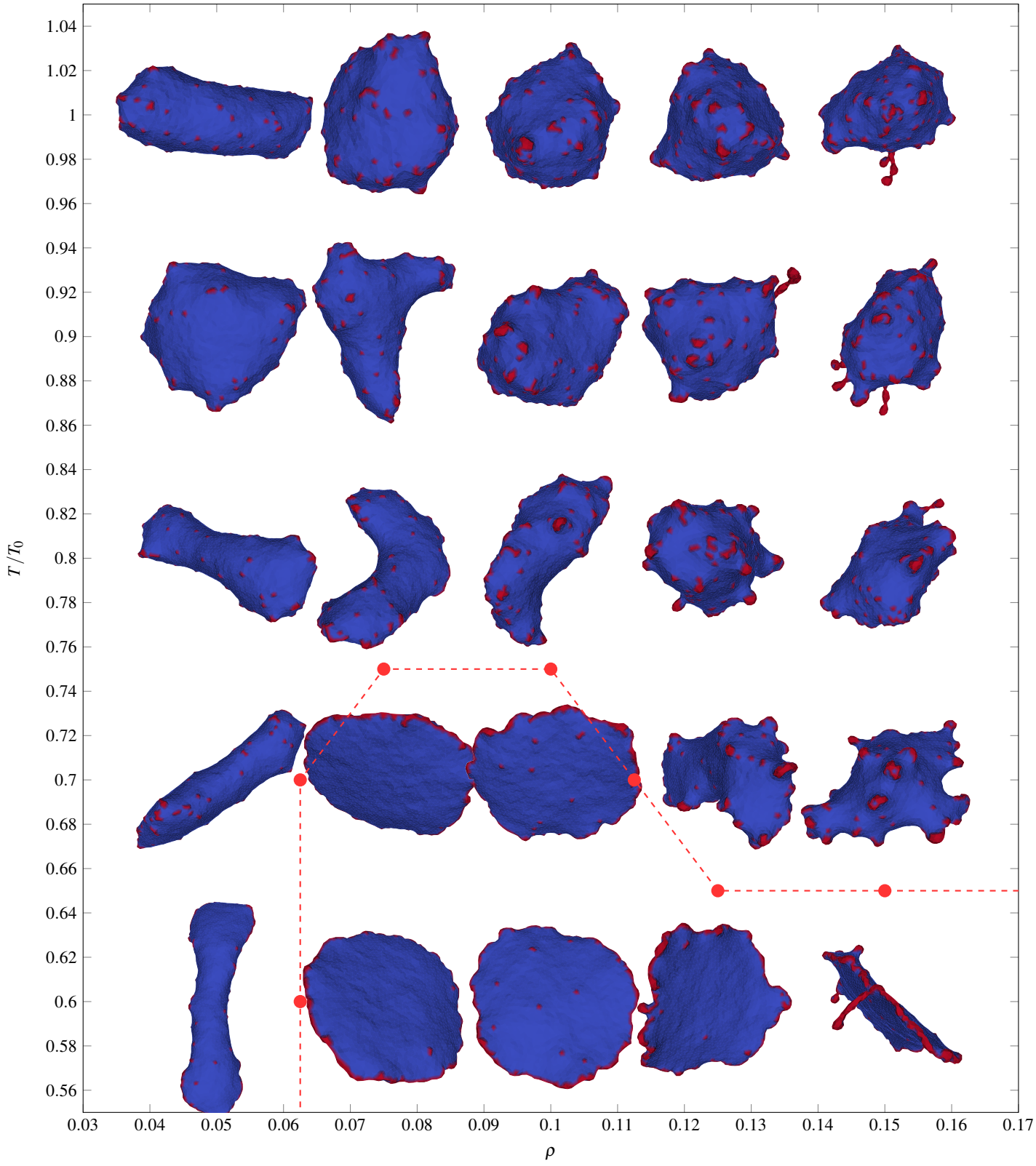

Figure S9 Representative snapshots of the vesicle at protein densities $\rho = 5$, 7.5, 10, 12.5 and 15% and temperatures $T/T_0 = 0.6$, 0.7, 0.8, 0.9 and 1.0, for $p = 0.005\,kT/l_{\text{min}}^3$ (with $k_A = 1\,kT_0$, $w = 1\ kT_0$ and $F = 1\,kT_0/l_{min}$). Approximate temperatures below which a transition into a pancake-like shapes is observed are indicated with red dots connected with dashed lines.

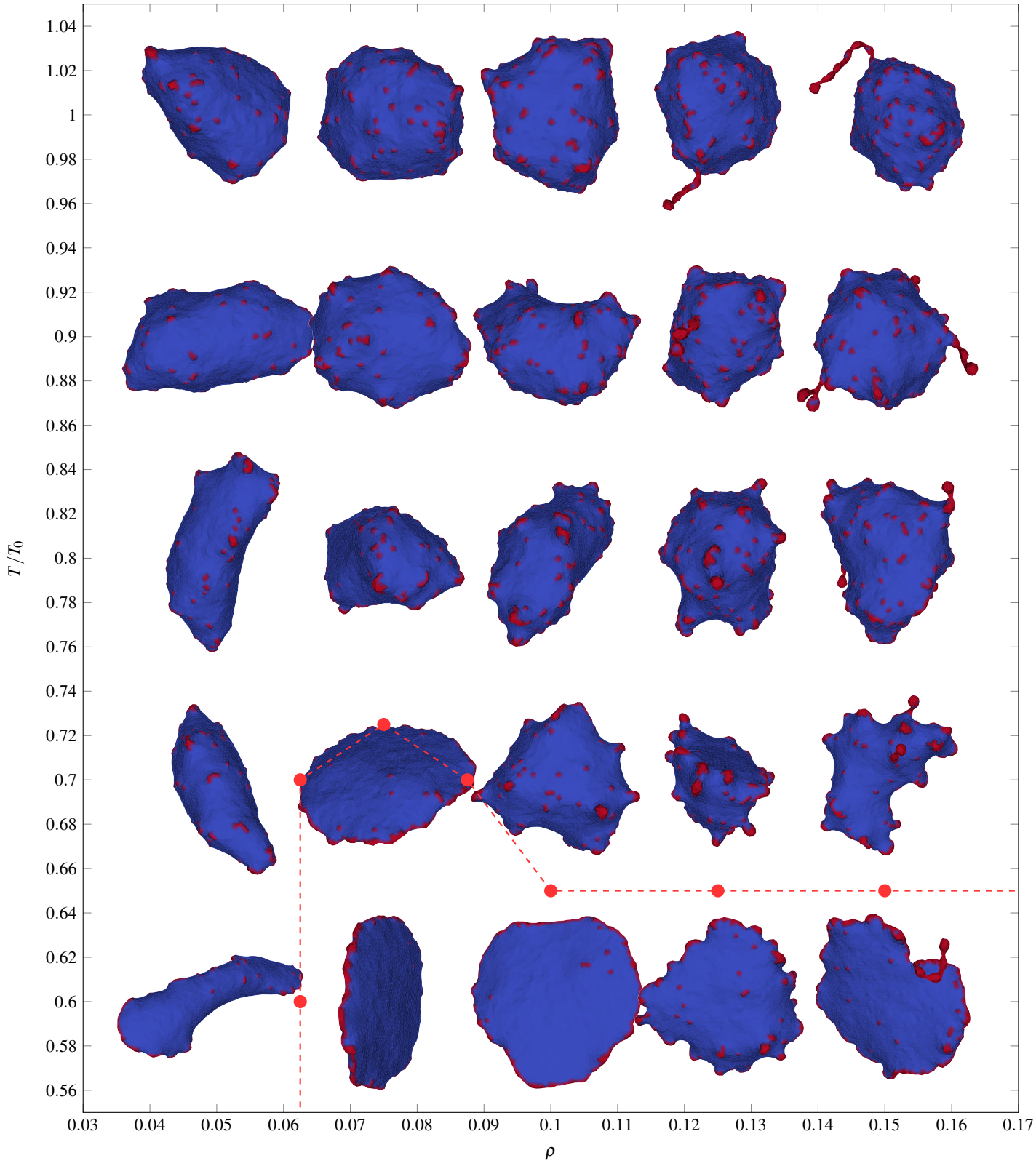

Figure S10 Representative snapshots of the vesicle at protein densities $\rho = 5$, 7.5, 10, 12.5 and 15% and temperatures $T/T_0 = 0.6$, 0.7, 0.8, 0.9 and 1.0, for $p = 0.01\,kT/l^3_{\text{min}}$ (with $k_A = 1\,kT_0$, $w = 1\,kT_0$ and $F = 1\,kT_0/l_{min}$). Approximate temperatures below which a transition into a pancake-like shapes is observed are indicated with red dots connected with dashed lines.

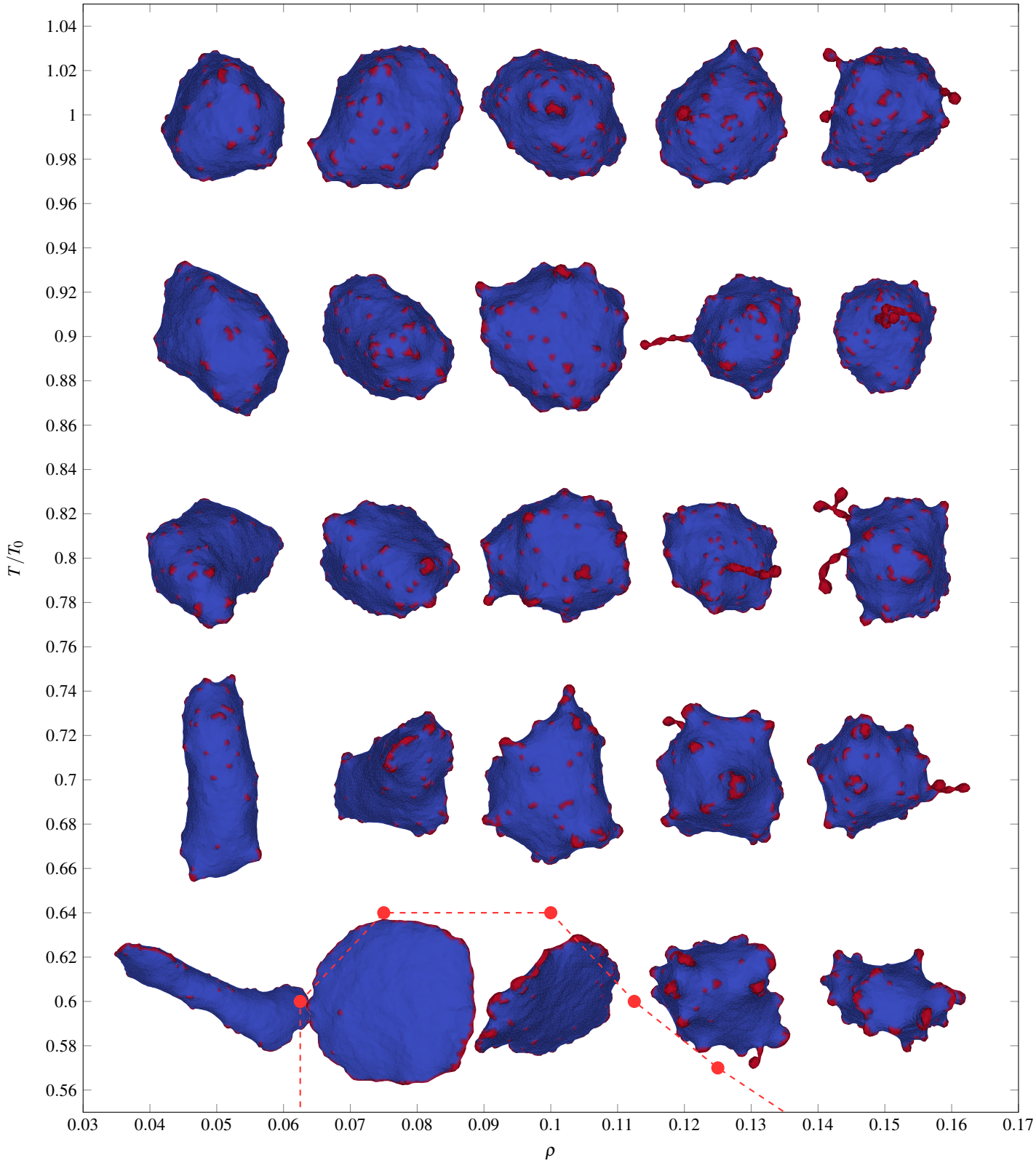

Figure S11 Representative snapshots of the vesicle at protein densities $\rho = 5$, 7.5, 10, 12.5 and 15% and temperatures $T/T_0 = 0.6$, 0.7, 0.8, 0.9 and 1.0, for $p = 0.015 kT/l_{\text{min}}^3$ (with $k_A = 1 kT_0$, $w = 1\ kT_0$ and $F = 1 kT_0/l_{min}$). Approximate temperatures below which a transition into a pancake-like shapes is observed are indicated with red dots connected with dashed lines.

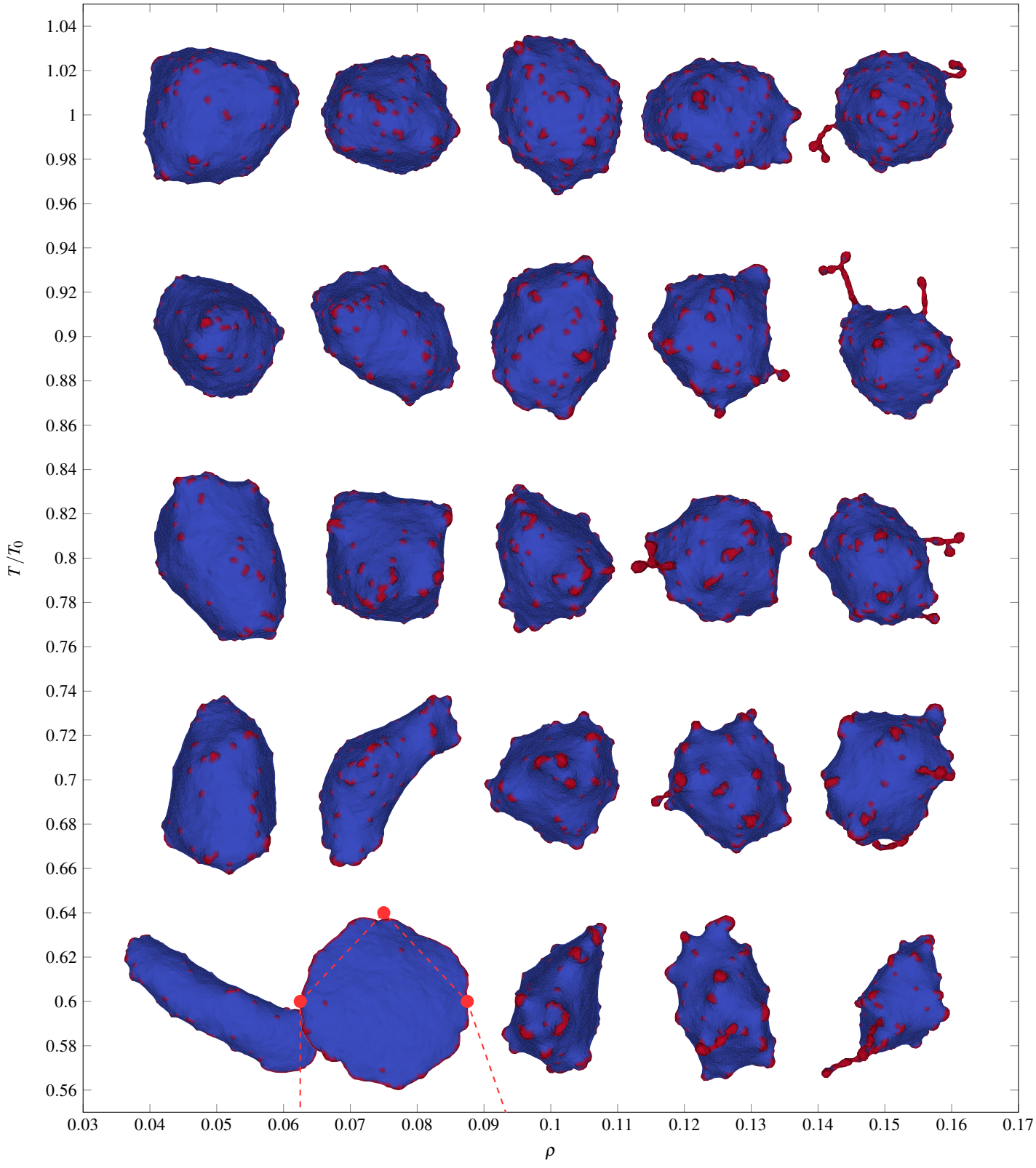

Figure S12 Representative snapshots of the vesicle at protein densities $\rho = 5$, 7.5, 10, 12.5 and 15% and temperatures $T/T_0 = 0.6$, 0.7, 0.8, 0.9 and 1.0, for $p = 0.02kT/l^3_{\text{min}}$ (with $k_A = 1\,kT_0$, $w = 1\,kT_0$ and $F = 1\,kT_0/l_{min}$). Approximate temperatures below which a transition into a pancake-like shapes is observed are indicated with red dots connected with dashed lines.

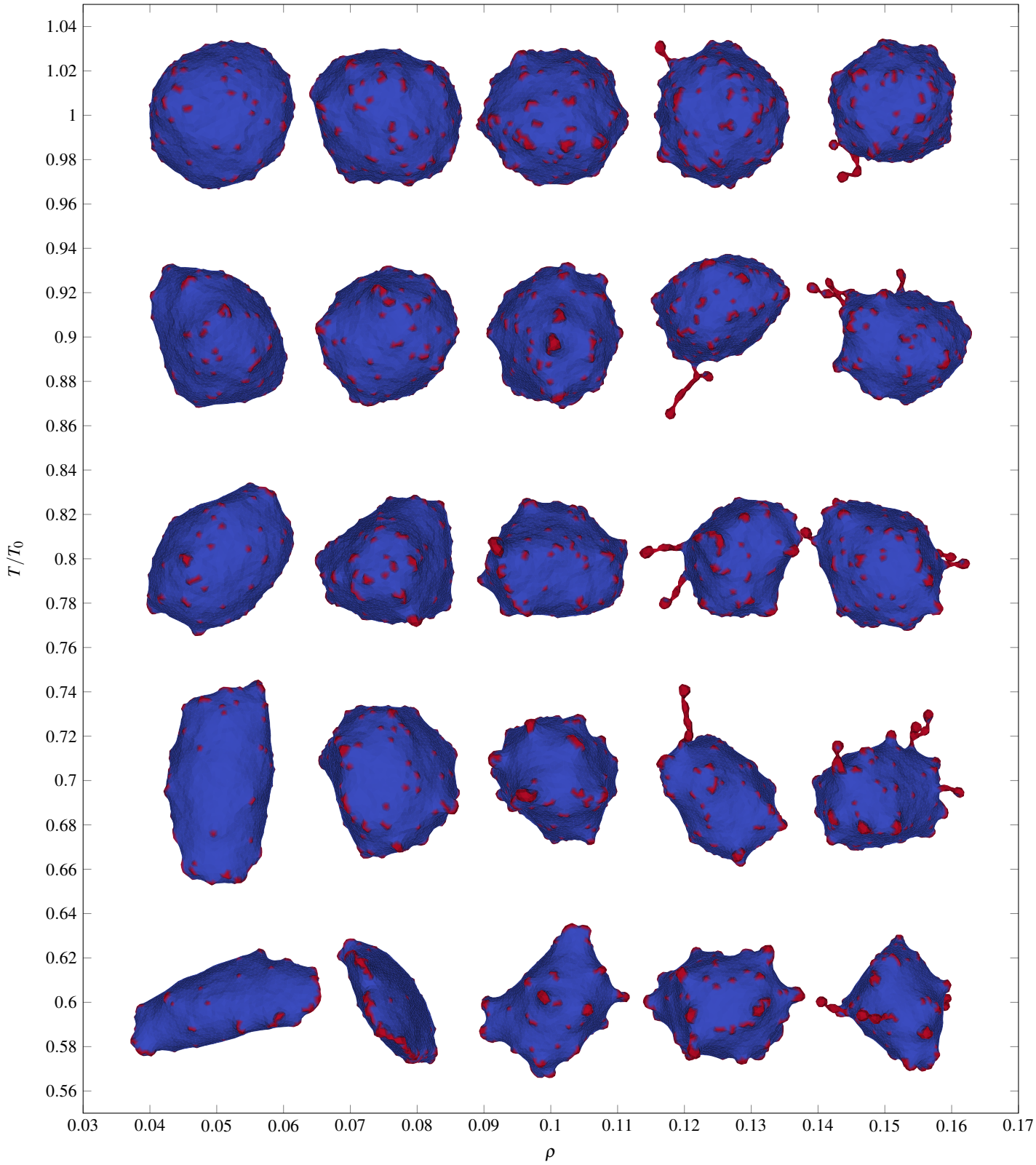

Figure S13 Representative snapshots of the vesicle at protein densities $\rho = 5$, 7.5, 10, 12.5 and 15% and temperatures $T/T_0 = 0.6$, 0.7, 0.8, 0.9 and 1.0, for $p = 0.025\,kT/l_{\text{min}}^3$ (with $k_A = 1\,kT_0$, $w = 1\ kT_0$ and $F = 1\,kT_0/l_{min}$).

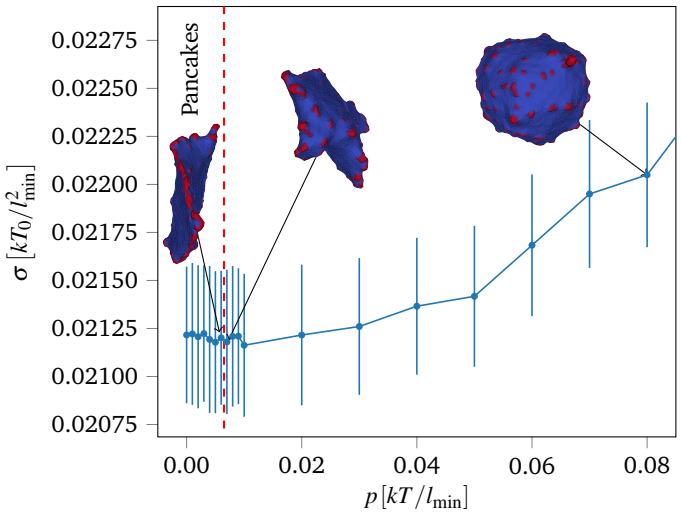

Figure S14 Membrane tension σ (Eq. S26) as a function of osmotic pressure p for a membrane with elastic constant (Eq. S25) $k_A = 1\,kT_0$, at temperature $T/T_0 = 0.7$, with $\rho = 11$ % of active proteins with direct interaction constant $w = 1\ kT_0$ and protrusive force $F = 1\ kT_0/l_{min}$. Averaging is done over 200 statistically independent microstates in steady state and error bars indicate standard deviations. Vertical dashed line indicates border of the pancake phase. Representative snapshots are shown for $p = 0.006kT/l_{\min}^3$ (pancake), $0.007\,kT/l_{\min}^3$ (protein rim disassembles and pancake shape is lost) and $0.08\,kT/l_{\min}^3$ (quasi-spherical shape).

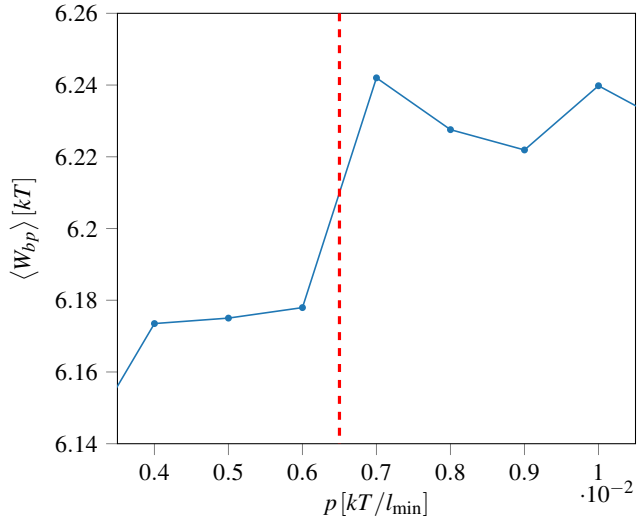

Figure S15 Ensemble averaged bending energy of proteins W_{bp} as a function of osmotic pressure near the border of the pancake phase (indicated by dashed vertical line), for a system used also in Fig. S14. Averaging is done over 400 statistically independent microstates in steady state.

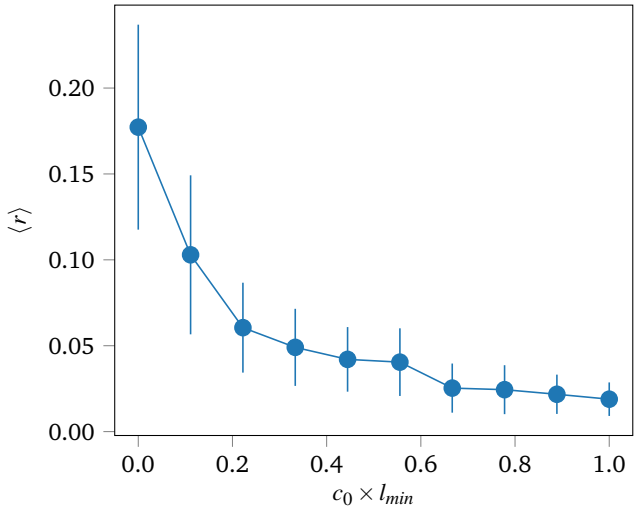

Figure S16 Ensemble average over 500 statistically uncorrelated microstates of the size of the normalized resultant of the protrusive forces (Eq. S27) as a function of the spontaneous curvature of active proteins, for $F = 1\,kT_0$, $w = 1\,kT_0$, $\rho = 11\%$ and $T/T_0 = 0.7$. As c_0 increases, the configurations go from hydra-like to pancake-like (see Fig. 7d in the main text). Error bars indicate standard deviations.

SI8: Normalized resultant of the protrusive forces

In our work we defined the local protrusive force due to the cytoskeleton at the active protein i as $\vec{F}_i = F\,\hat{n}_i$, where F is the size of the force and $\hat{n}_i$ is the outward facing normal to the membrane at the location of protein i (see Eq. 4 in the main text). Here we define the normalized resultant of the protrusive forces,

$$\vec{r} = \frac{\sum_i \hat{n}_i}{\sum_i |\hat{n}_i|} \tag{S27}$$

where the sums run over all proteins. Note that size of vector $\vec{r}$ is $r = |\vec{r}| = 0$ when the protrusive forces cancel out and the net protrusive force on the vesicle is zero, and $r = 1$ when all protrusive forces show in the same direction.

Fig. S16 shows the ensemble averaged r for different scenarios - pancake and hydra shapes. As we expected, pancake shapes have lower r than hydra shapes.

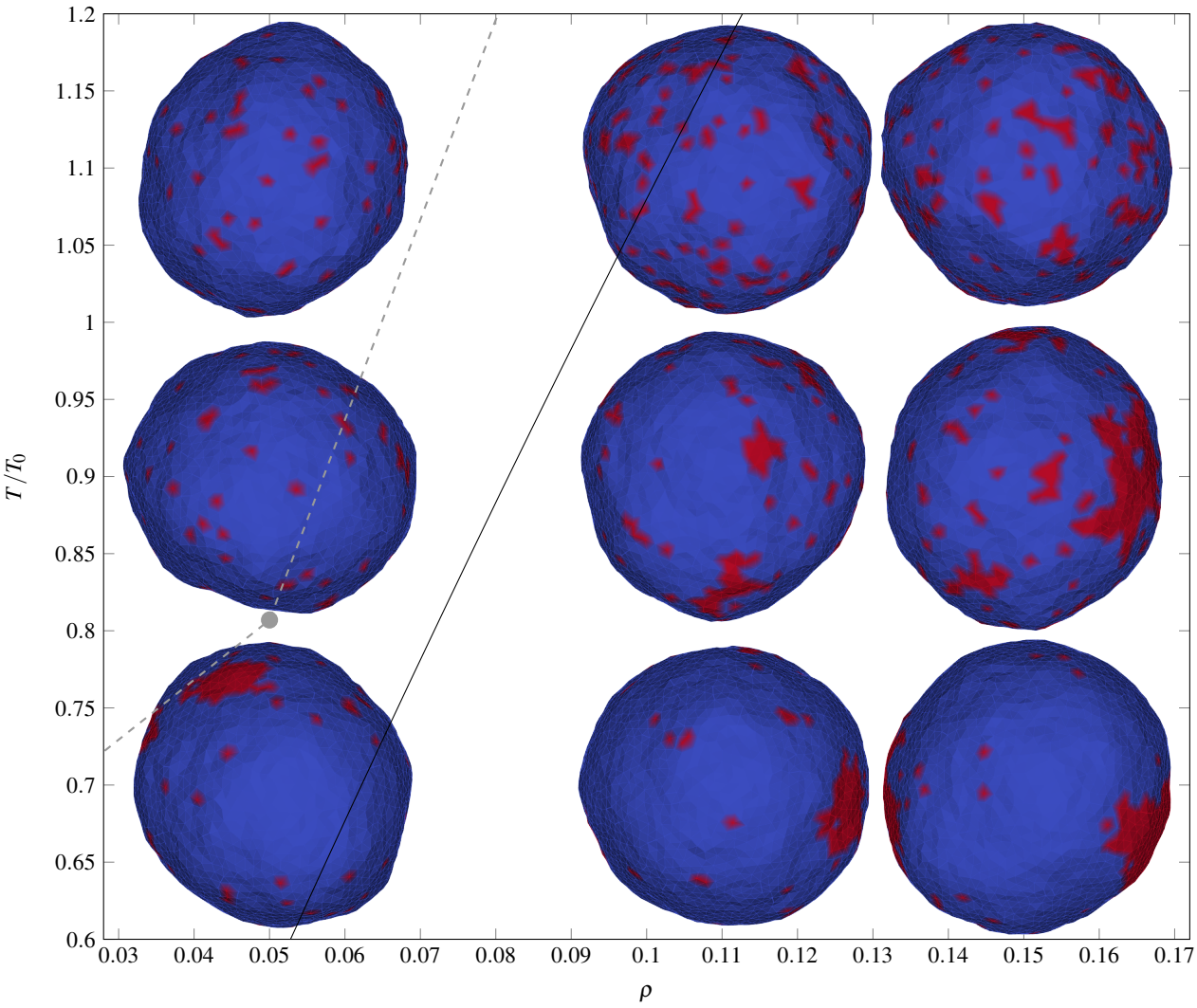

Figure S17 Representative snapshots for flat passive proteins with $w = 1\,kT_0$ for protein with densities $\rho = 0.05$, 0.11, 0.15 at temperatures $T/T_0 = 0.7$, 0.9, 1.1. Black solid curve denotes the prediction of the critical temperature by the linear stability analysis (Eq. 6). Gray point with dashed line denotes where $\langle \bar{N}_{\rm vc} \rangle = 2$ (for $\rho = 0.11$ and 0.15, $\langle \bar{N}_{\rm vc} \rangle > 2$ for all three temperatures shown).

SI9: Simulations with flat passive proteins

We also simulated membrane with flat passive proteins, where the only difference between vertices representing the proteins and the rest of the membrane is that the proteins feel the attractive direct interaction (Eq. 3).

In Fig. S17 we plot representative snapshots for different values of protein densities and temperatures. As expected, all shapes are quasi-spherical. There is only phase-separation due to direct protein-protein interactions.

MOVIES

Movie S1: Animation of snapshots in steady-state of the system with $\rho = 7\,\%$ of curved active proteins with $F = 1\,kT_0/l_{min}$, $c_0 = 1/l_{min}$, $w = 1\,kT_0$ at $T/T_0 = 0.6$ (see the last snapshot in the second line from below on Fig. 5a).

Movie S2: Animation of snapshots in steady-state of the system with $\rho = 5\,\%$ of curved active proteins with $F = 1\,kT_0/l_{min}$, $c_0 = 1/l_{min}$, $w = 1\,kT_0$ at $T/T_0 = 0.6$ (see the second snapshot in the second line from below on Fig. 5a).

Movie S3: Animation of snapshots in steady-state of the system with $\rho = 11\,\%$ of almost flat active proteins with $F = 1\,kT_0/l_{min}$, $c_0 = 1/(9l_{min})$, $w = 1\,kT_0$ at $T/T_0 = 0.7$ (see the top-left shape on Fig. 7d).

Movie S4: Animation of snapshots in steady-state of the system for osmotic pressure $p = 0.006\,kT/l_{\mathrm{min}}^3$ with $k_A = 1\,kT_0$, at temperature $T/T_0 = 0.7$, with $\rho = 11$ % of active proteins with direct interaction constant $w = 1\ kT_0$ and protrusive force $F = 1\ kT_0/l_{min}$ (see Fig. S14).

Movie S5: Animation of snapshots in steady-state of the system for osmotic pressure $p = 0.007\,kT/l_{\mathrm{min}}^3$ with $k_A = 1\,kT_0$, at temperature $T/T_0 = 0.7$, with $\rho = 11$ % of active proteins with direct interaction constant $w = 1\ kT_0$ and protrusive force $F = 1\ kT_0/l_{min}$ (see Fig. S14).

Movie S6: Animation of snapshots in steady-state of the system with $\kappa = 20kT_0$, $T/T_0 = 0.7$, $\rho = 11\%$, $w = 1\,kT_0$ (see Fig. 7d, green dots) and $c_0 = 1/(9l_{min})$ (top left shape on Fig. 7d, and movie S3), but with a patch of seven vertices fixed in space (denoted with green boxes).

Movie S7: Animation of snapshots in steady-state of the system with $\kappa = 20kT_0$, $T/T_0 = 0.7$, $\rho = 11\%$, $w = 1\,kT_0$ (see Fig. 7d, green dots) and $c_0 = 1/l_{min}$, but with a patch of seven vertices fixed in space (denoted with green boxes).